Journal of Materials Chemistry A

PAPER

View Article Online
View Journal | View Issue

Cite this: J. Mater. Chem. A, 2015, 3, 12777

Lanthanide metal–organic frameworks containing a novel flexible ligand for luminescence sensing of small organic molecules and selective adsorption†

Xiaoqing Wang,[b] Liangliang Zhang,[a] Jie Yang,[b] Fuling Liu,[b] Fangna Dai,[a] Rongming Wang[a] and Daofeng Sun*[ab]

Received 5th January 2015
Accepted 3rd May 2015

DOI: 10.1039/c5ta00061k

www.rsc.org/MaterialsA

Five lanthanide metal–organic frameworks, [Ln(L)(H$_2$O)(NMP)]·1.5H$_2$O (Ln = Ce (**1**), Pr (**2**); H$_3$L = 1,3,5-tris(4-carboxyphenyl-1-ylmethyl)-2,4,6-trimethylbenzene), and [Ln$_2$(L)$_2$(H$_2$O)$_3$]·2H$_2$O (Ln = Eu (**3**), Tm (**4**), Yb (**5**)), have been synthesized and characterized. Complexes **1–5** exhibit similar 1D channels through the linkage of Ln-carboxylate chains with the backbones of H$_3$L ligands. The channels for complexes **1** and **2** are occupied by coordinated NMP molecules. **3** shows potential application for the luminescence sensing of small organic molecules. Moreover, **5** exhibits selective adsorption of CO_2 over N_2 and CH_4 and catalytic activities toward the cyanosilylation reaction.

Introduction

Currently, environmental issues have been attracting considerable attention from governments and scientists, which are mainly focused on air, water, and industrial-waste pollution due to the detriment caused to sustainable development and human health. How to solve the pollution problem has become one of the hottest topics worldwide. Plenty of money and manpower has been invested, but technique-based instruments for detecting pollution are not always available. Thus, there is an urgent need to develop a novel method that can be applied to various pollutants.

Metal–organic frameworks (MOFs), which are assembled by metal ions/clusters and organic ligands, have gathered considerable attention over recent decades as a new frontier for material research.[1–3] Their fascinating topology, high surface areas and well-defined porosity make them suitable for potential applications such as gas storage and separation,[4–6] luminescence,[7–9] electronics,[10–12] drug delivery,[13–15] and catalysis.[16–19] To obtain predictable structures and excellent properties, numerous research studies have been reported for constructing novel MOFs by the reasonable selection of organic linkers and functional metal ions.[20–23] As a sub-family of MOFs, lanthanide MOFs (Ln-MOFs) have been studied widely for their unique physical properties, which exhibit interesting photophysical, magnetic, and electronic properties originating from 4f electrons.[24–28] Compared with d-block transition metal ions, lanthanide ions have high and variable coordination numbers, and flexible coordination environments. At present, various MOFs have been used for environmental protection.[29] The emission of carbon dioxide (CO_2) causes the global greenhouse effect as the main motivation, and using MOFs for CO_2 storage has received considerable attention for potential applications due to their permanent porosity, ex-high surface areas, and adjustable pore sizes and shapes.[30–35] Moreover, Ln-MOFs as fluorescent probes can be used in the recognition and sensing of small organic molecules for their important roles in environmental systems.[36,37] In particular, lanthanide ions, Eu^{3+} and Tb^{3+}, are receiving increasing attention because of their exceptional luminescent features, such as long luminescence lifetimes, sharp pure red and green emission, and large Stokes shift values.[38–44]

In the past few decades, various Ln-MOFs have been constructed using different organic linkers.[45–49] As is well-known, aromatic multicarboxylate ligands are widely used in the architecture for Ln-MOFs because Ln ions have high affinity for oxygen atoms on the carboxylate. Since the use of 1,3,5-benzenetricarboxylates by Yaghi's group to construct a 3D Ln-MOF,[49] which is robust and contains 1D rod-shaped Ln-carboxylate chains as secondary building units (SBUs), many 3D rod-packing Ln-MOFs have been synthesized and their potential applications in gas adsorption have been subsequently studied.[50–55] However, this synthetic strategy is mainly focused on the rigid ligands with single conformations. The Ln-MOFs constructed by flexible ligands are less investigated.[56–59] On the one hand, compared with rigid ligands, flexible ligands have various coordination modes and the final structures are hard to predict. On the other hand, flexible ligands have gained

[a]State Key Laboratory of Heavy Oil Processing, China University of Petroleum (East China), College of Science, China University of Petroleum (East China), Qingdao, Shandong, 266580, People's Republic of China. E-mail: dfsun@upc.edu.cn

[b]Key Lab of Colloid and Interface Chemistry, Ministry of Education, School of Chemistry and Chemical Engineering, Shandong University, Jinan, Shandong, 250100, People's Republic of China

† Electronic supplementary information (ESI) available. CCDC 1035915–1035919. For ESI and crystallographic data in CIF or other electronic format see DOI: 10.1039/c5ta00061k

considerable attention for the construction of porous coordination polymers because the assembled products possess several unique advantages such as breathing ability and adaptive recognition properties. Therefore, it is significant to assemble preferred Ln-MOFs using flexible organic ligands.

Based on the abovementioned consideration, we designed and synthesized a novel flexible ligand, 1,3,5-tris(4-carboxyphenyl-1-ylmethyl)-2,4,6-trimethylbenzene (H_3**L**). It holds flexibility due to the presence of a –CH_2– spacer, which can meet the requirement of various coordination conformations. On the basis of this ligand, five Ln-MOFs (Ln = Ce, Pr, Eu, Tm, Yb) based on rod-shaped SBUs have been synthesized, which exhibit two different structure types: [Ln(**L**)(H_2O)(NMP)]·1.5H_2O (Ln = Ce (**1**), Pr (**2**)) and [Ln_2(**L**)$_2$(H_2O)$_3$]·2H_2O (Ln = Eu (**3**), Tm (**4**), Yb (**5**)). The luminescent properties of complexes **1–5** were investigated, and complex **3** was found to exhibit an interesting sensing property for small organic molecules such as acetone and aromatic compounds. In addition, complex **5** with large 1D channels was characterized by detailed CO_2 adsorption and separation exploration, as well as the study of catalytic properties.

Experimental

Materials and methods

All the materials were purchased and used without further purification. The ligand H_3**L** was synthesized in 60% yield by a Pd-catayzed Suzuki coupling reaction between 1,3,5-tris-(bromomethyl)-2,4,6-trimethylbenzene and 4-methoxycarbonylphenylboronic followed by hydrolysis with dilute HCl, which was characterized by ^{1}H NMR (please see the ESI†). Thermo-gravimetric analysis (TGA) experiments were carried out on a Mettler Toledo TGA instrument with a heating rate of 10 °C min^{-1} in the range of 25–800 °C under a N_2 atmosphere. Elemental analyses (C, H, and N) were performed on a CE instrument EA 1110 elemental analyzer. IR spectra were obtained on a Nexus FT-IR Spectrometer within the 4000–500 cm^{-1} region. The powder XRD data were obtained on an X-Pert PRO MPD diffractometer with Cu-Kα radiation. Photoluminescence spectra were recorded using a Hitachi F-7000 Fluorescence Spectrophotometer. Gas-sorption isotherms were carried out on a surface area analyzer, ASAP-2020.

Synthesis of MOFs

A mixture of H_3**L** (2 mg, 0.0037 mmol), $Ce(NO_3)_3·6H_2O$ (5 mg, 0.012 mmol), H_2O/HNO_3 (0.02 mL, v/v, 20/1) and H_2O/1-methyl-2-pyrrolidone (NMP) (l mL, v/v, 1/1) was heated to 120 °C for 3000 min in a sealed tube. The colorless crystals were collected by filtration, washed with EtOH and dried in air. Complexes **2–5** were synthesized by a similar procedure using $Ln(NO_3)_3·6H_2O$ (Ln = Pr, Eu, Tm, Yb).

[Ce(L)(H_2O)(NMP)]·1.5H_2O (1). Yield: 25%. Anal. calcd for **1**: C, 56.73; H, 5.10; N, 1.74. Found: C, 56.45; H, 5.19; N 1.82%. IR (KBr, cm^{-1}): 3442 (m), 2917 (w), 1657 (m), 1587 (m), 1538 (m), 1403 (s), 765 (m).

[Pr(L)(H_2O)(NMP)]·1.5H_2O (2). Yield: 21%. Anal. calcd for **2**: C, 59.47; H, 4.96; N, 1.83. Found: C, 59.51; H, 4.93; N 1.89%. IR (KBr, cm^{-1}): 3404 (m), 2934 (m), 1662 (m), 1592 (m), 1538 (m), 1403 (s), 1014 (m), 760 (m).

[Eu_2(L)$_2$(H_2O)$_3$]·2H_2O (3). Yield: 19%. Anal. calcd for **3**: C, 55.27; H, 4.47. Found: C, 55.18; H, 4.42%. IR (KBr, cm^{-1}): 3436 (m), 2928 (w), 1647 (w), 1603 (m), 1544 (m), 1425 (s), 1014 (m), 765 (m).

[Tm_2(L)$_2$(H_2O)$_3$]·2H_2O (4). Yield: 23%. Anal. calcd for **4**: C, 53.99; H, 4.36. Found: C, 53.95; H, 4.42%. IR (KBr, cm^{-1}): 3376 (m), 2934 (w), 1652 (w), 1603 (m), 1554 (m), 1420 (s), 1020 (m), 765 (m).

[Yb_2(L)$_2$(H_2O)$_3$]·2H_2O (5). Yield: 40%. Anal. calcd for **5**: C, 53.69; H, 4.34. Found: C, 53.66; H, 4.30%. IR (KBr, cm^{-1}): 3404 (m), 2928 (w), 1652 (w), 1603 (m), 1549 (m), 1414 (s), 1020 (m), 760 (m).

X-ray structure determination and structure refinement

The X-ray intensity data of the complexes **1–5** were collected on an Agilent Xcalibur Eos Gemini diffractometer with Cu Kα radiation (λ = 1.54178 Å) at 293 K. An empirical absorption correction was used *via* the multi-scan method. Data reduction was corrected for Lorentz, polarization and absorption effects. In all the cases, the highest possible space group was chosen. Structures were solved by the direct method with *SHELXL-97* and refined by full-matrix least-squares on F^2 using *SHELXL-97*.[60] Non-hydrogen atoms were refined anisotropically. Hydrogen atoms were placed in calculated positions and refined as riding atoms with isotropic displacement parameters 1.2–1.5 times U_{eq} of the attached atoms. For complexes **3–5**, there are large solvent accessible void volumes, where many disordered NMP and water molecules exist. However, no satisfactory disorder model could be achieved; thus, these electron densities can be removed by *PLATON/SQUEEZE*.[61] Table 1 presents their crystallographic data collection and refinement parameters. Table S1 displays the selected bond distances and angles (ESI†).

Results and discussion

Description of the crystal structures

Since complexes **1–2** are isostructural, the structure of complex **1** is discussed as an example. X-ray single-crystal diffraction analysis reveals that complex **1** possesses a neutral three-dimensional (3D) metal–organic framework. Complex **1** crystallizes in the triclinic space group $P\bar{1}$. The asymmetric unit contains one Ce(III) ion, one L^{3-} ligand, one coordinated NMP molecule and one coordinated water molecule. As shown in Fig. 1a, the central Ce1 is eight-coordinated by six oxygen atoms from different L^{3-} ligands, one oxygen atom from the coordinated NMP molecule, and one oxygen atom from the coordinated H_2O molecule, and shows a distorted square antiprism coordination geometry. The Ce–O bond distances range from 2.418 Å to 2.616 Å and O–Ce–O bond angles range from 68.04 Å to 149.25 Å. All the bond lengths and bond angles are consistent with the previously reported results.[62–64] Scheme S1† shows the

Table 1 Crystal data for complexes **1–5**

Complexes	**1**	**2**	**3**	**4**	**5**
Formula	$C_{38}H_{38}CeNO_8$	$C_{38}H_{38}PrNO_8$	$C_{66}H_{60}Eu_2O_{15}$	$C_{66}H_{60}Tm_2O_{15}$	$C_{66}H_{60}Yb_2O_{15}$
M_r	776.81	739.80	1397.08	1430.98	1439.17
Crystal system	Triclinic	Triclinic	Orthorhombic	Orthorhombic	Orthorhombic
Space group	$P\bar{1}$	$P\bar{1}$	*Pnma*	*Pnma*	*Pnma*
a (Å)	9.8401(3)	9.8432(3)	32.8077(5)	32.8303(7)	32.7626(14)
b (Å)	10.0517(3)	10.0408(3)	35.0306(5)	34.9113(8)	34.950(2)
c (Å)	18.0642(6)	18.0453(7)	5.73210(15)	5.8318(2)	5.7721(4)
α (deg)	90.221(3)	90.135(3)	90.00	90.00	90.00
β (deg)	93.857(3)	93.963(3)	90.00	90.00	90.00
γ (deg)	113.891(3)	113.872(3)	90.00	90.00	90.00
Z	2	2	4	4	4
V (Å^3)	1628.99(10)	1626.10(10)	6587.8(2)	6684.1(3)	6609.3(7)
D_c (g cm^{-3})	1.584	1.511	1.402	1.420	1.440
μ (mm^{-1})	11.264	11.958	13.997	2.698	5.600
F (000)	790.0	717.0	2784.0	2848.0	2840.0
No. of unique reflns	11 011	10 338	23 642	13 416	13 741
No. of obsd reflns [$I > 2\sigma(I)$]	5791	5124	6295	5968	6250
Parameters	444	437	355	385	382
GOF	1.107	1.067	1.093	1.140	1.183
Final R indices [$I > 2\sigma(I)$][a,b]	$R_1 = 0.0363$	$R_1 = 0.1042$	$R_1 = 0.1415$	$R_1 = 0.1147$	$R_1 = 0.1249$
	$wR_2 = 0.1021$	$wR_2 = 0.2893$	$wR_2 = 0.3691$	$wR_2 = 0.3191$	$wR_2 = 0.3355$
R indices (all data)	$R_1 = 0.0370$	$R_1 = 0.1085$	$R_1 = 0.1724$	$R_1 = 0.1383$	$R_1 = 0.1590$
	$wR_2 = 0.1026$	$wR_2 = 0.2919$	$wR_2 = 0.3963$	$wR_2 = 0.3420$	$wR_2 = 0.3661$

[a] $R_1 = \sum||F_o| - |F_c||/\sum|F_o|$. [b] $wR_2 = [\sum w(F_o^2 - F_c^2)^2/\sum w(F_o^2)^2]^{0.5}$.

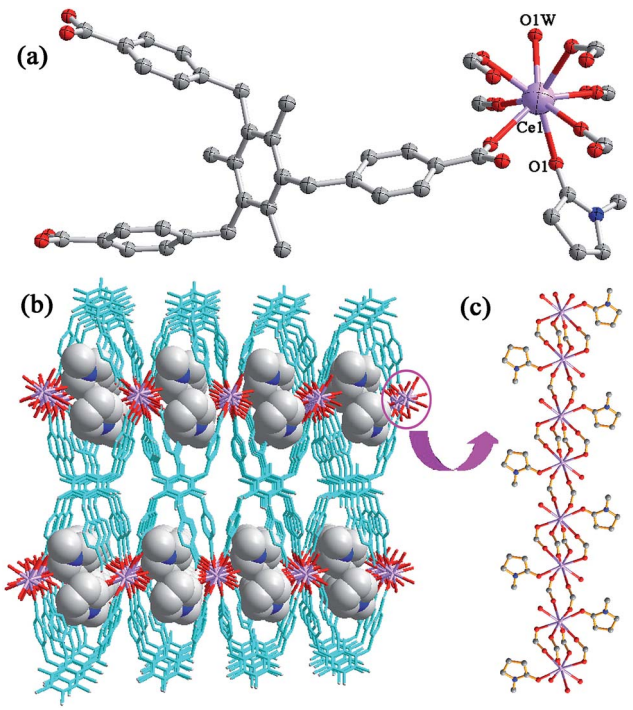

Fig. 1 (a) Coordination environment of the Ce atom in **1**. (b) Projection view of the framework **1** along the *b* axis with coordinated NMP in the highlighted channels. (c) The 1D rod-shape SBU in complex **1**.

coordination modes of the L^{3-} ligand. For **1**, L^{3-} exhibits the same coordination mode as A: μ_6-η^1: η^1: η^1: η^1: η^1, and each carboxyl group bridges two Ce(III) ions.

In complex **1**, two crystallographically equivalent Ce atoms are bridged by four carboxyl groups to obtain a binuclear block. The interlinkage between $Ce_2(CO_2)_4$ clusters and the carboxylate group of L^{3-} generates 1D infinite rod-shape Ce-carboxylate chains along the *b* axis, which are further linked by the backbones of L^{3-} to construct a 3D framework (Fig. 1b and c). Similar Ln-carboxylate rod-shaped SBUs have also been reported previously.[65–68] Along the *b* axis, the 3D framework contains narrow 1D rhombic channels with a side length of ~9.18 Å, which are occupied by coordinated NMP molecules (Fig. 1b). To further study the nature of the intricate framework, its topology was analyzed using a free computer program *TOPOs*.[69] Herein, each ligand binds four neighboring binuclear $Ce_2(CO_2)_4$ clusters, and each binuclear cluster is linked by eight neighboring L^{3-} ligands. Thus, the structure can be simplified as a 4, 8-connected net of type fluorite (sqc 169) with the point symbols $\{4^{12}.6^{12}.8^4\}$ and $\{4^6\}$ (Fig. S1†).

X-ray single-crystal diffraction analysis reveals that complexes **3–5** are also isostructural, which crystallize in the orthorhombic, space group of *Pnma*. We chose the structure of **4** as an example. The asymmetric unit of **4** consists of half Tm1 ion, half Tm2 ion, one L^{3-} anion, and three halves of coordinated H_2O molecules. Two metal centers of Tm(III) are both located on one mirror symmetry. As depicted in Fig. 2a, there are two independent Tm(III) ions in **4**. Tm1 is seven-coordinated by six carboxylate oxygen atoms from the L^{3-} ligand and one oxygen atom from a coordinated H_2O molecule with Tm1–O bond distances from 2.200(10) Å to 2.504(19) Å. Tm2 exhibits a distorted square antiprism coordination geometry completed by six oxygen atoms from four different L^{3-} ligands, and two oxygen atoms from

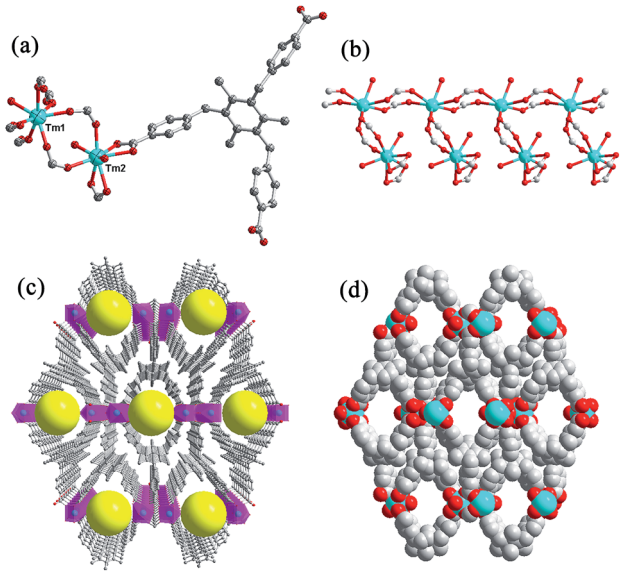

Fig. 2 (a) Coordination environment of Tm atom in **4**. (b) The 1D rod-shaped SBU in **4**. (c) Projection view of the framework **4** along the *c* axis, showing the rhombic channels. (d) 3D porous framework shown in the space-filling mode.

coordinated H_2O molecules (bond lengths of Tm2–O are within the range of 2.258 Å to 2.406 Å). Here, the coordination mode of the L^{3-} ligand is μ_5-η^2: η^1: η^1: η^1, which is different from those in complexes **1** and **2** (Scheme S1†).

As shown in Fig. 2b, the binuclear Tm clusters are connected to each other by two carboxylate groups to form 1D infinite rod-shaped SBU along the *c* axis. The 1D chains are further linked by L^{3-} ligands to form a porous 3D MOF, which contains a rhombic channel viewed from the *c* axis with the window sizes of 13.7 Å × 6 Å (Fig. 2c and d). The void volume calculated by *PLATON* is 13.9%, which are occupied by disorder solvent molecules.[70] Topologically, the binuclear Tm cluster can be treated as an eight-connected node. Since one L^{3-} ligand connects four binuclear Tm clusters, the L^{3-} ligand can be simplified as a four-connected node, and the whole framework forms a 4, 8-connected net of alb-4,8-*Pnma* (binodal.ttd) type with the point symbols $\{4^5.6\}^2$ $\{4^7.6^{20}.8\}$ (Fig. S2†).[69]

Effect of lanthanide contraction and the coordination modes of organic ligands on the structure

Although complexes **1–5** were synthesized by the same experimental method, they exhibit two distinct structure types. This may be caused by two reasons: lanthanide contraction and the coordination modes of the organic ligand. Generally, the smaller the sizes of Ln(III) ions, the greater the repulsions among the coordination atoms around the central metal.[71,72] The repulsions cause the crystal structure to become unstable and a new structure is formed. The light Ln(III) ions could form higher coordinated geometry numbers than the heavy Ln(III) ion. As shown in Fig. 3, it is obvious that the average Ln–O bond length decreases with the decrease of ionic radii of the Ln(III) ions and the bond lengths in complexes **1–2** are considerably

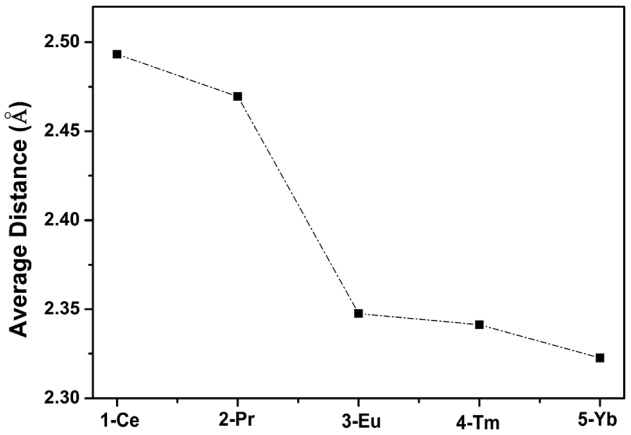

Fig. 3 Variation of the average Ln–O distance in **1–5**.

larger than those in complexes **3–5**. The decreases cause the increasing repulsions among the coordinated atoms and the crystal structure becomes unstable. The coordination numbers of Ln(III) ions present the tendency of decreasing (from eight for complexes **1–2** to seven for complexes **3–5**). In addition, it is worth noting that the coordination modes of the L^{3-} ligand for two types of structures are different (Scheme S1†). In complexes **1–2**, each carboxylate group of L^{3-} adopts a bidentate bridging coordination mode, while in complexes **3–5**, there exists two types of coordination arrangements: bidentate bridging and bis-chelating coordination modes. Thus, both the lanthanide contraction and the coordination modes of the organic ligand have a significant effect on the structures of Ln-coordination complexes in this work.

Thermogravimetric analyses, IR spectra and X-ray powder diffraction analyses

To study the stability of complexes **1–5**, thermogravimetric analyses (TGA) were carried out from 25 to 800 °C under a dry nitrogen atmosphere. The isomorphous structures showed similar TGA curves; thus, we chose complexes **1** (Ce) and **5** (Yb) as representative examples to discuss their stability (Fig. S3†). The TGA curve of **1** shows a weight loss of 3.1% from 91 to 160 °C corresponding to the loss of lattice H_2O molecules (calcd: 3.3%). A plateau is observed till 282 °C. Subsequently, a weight loss of 13.1% occurs between 282 and 481 °C, which corresponds to the loss of coordinated H_2O and NMP molecules (calcd: 14.5%). Then, complex **1** starts to decompose above 485 °C. For complex **5**, in the range of 49–152 °C, the first weight loss is 2.1%, which corresponds to the loss of uncoordinated H_2O molecules (calcd: 2.3%). The weight loss of 5.0% between 236 and 394 °C is attributed to the loss of coordinated H_2O molecules (calcd: 3.7%). Beyond 480 °C, a rapid weight loss is observed, which indicates the decomposition of complex **5**. The TGA curves of **1–5** demonstrate the high stabilities, which is attributed to the existence of 1D infinite SBUs in the structures.

The IR spectrum and experimental powder XRD diffraction for complexes **1–5** are shown in Fig. S4 and S5,† respectively. The

experimental powder XRD patterns are almost identical to the corresponding simulated ones, indicating that the phase is pure.

Luminescent property and sensing of small organic molecules

The solid-state emission spectra of the free ligand H_3**L** and five samples **1–5** were measured at room temperature (Fig. 4). The absorption spectrum of H_3**L** displays a maximum peak at 427 nm (λ_{ex} = 298 nm), which originates from the $\pi\cdots\pi^*$ transition.[73,74] The emission peaks of the lanthanide complexes **1**, **2**, **4** and **5** (Ln = Ce, Pr, Tm, Yb) resemble that of H_3**L**, indicating that $\mathbf{L}^{3-}$ sensitizes Ln ions *via* the antenna effect and their emissions are attributed to the $\pi^*\cdots\pi$ transitions modified by metal coordination.[62,75–77] In addition, the emission spectrum of the Eu^{3+} complex exhibits the characteristic transitions of the Eu^{3+} energy-level structure at 592, 616, 652 and 701 nm.[78–80] This can be attributed to the transitions between the $^7F_0$ and the $^5L_6$ and $^5D_2$ levels. The sharp line characteristic indicates the inefficient sensitization of Eu^{3+} ions *via* the excitation of the ligand. Obviously, the emission intensities at 592 and 616 nm are stronger, which arise from the $^5D_0 \rightarrow {}^7F_1$ and $^5D_0 \rightarrow {}^7F_2$ transitions, respectively. They can be used to measure the coordination state and the site symmetry of the Eu^{3+} ion. The former transition is magnetic dipole and insensitive to the coordination environment, while the latter is electric dipole, and its intensity increases with decreasing site symmetry. In the spectrum of the Eu^{3+} complex, the former intensity is weaker than the latter, indicating the absence of inversion symmetry at the Eu^{3+} site.

As is well-known, fluorescent MOF materials as a useful chemical sensor are sensitive to some guest solvent molecules.[36,37] The characteristic luminescence of complex **3** prompted us to examine the potential for sensing small organic solvent molecules. For the luminescent sensing study, finely ground samples of **3** were dispersed in various organic solvents (DMSO, DMF, acetone, i-PrOH, cyclohexane, benzene, and toluene), and then treated by ultrasonication for 30 min. As shown in Fig. 5a and b, the intensities of **3** in the PL spectra strongly depend on the solvent molecules. Notably, acetone exhibits the most significant quenching effect. To further investigate the quenching effect of acetone on the luminescent intensity of **3**, equivalent aliquots of **3** were dispersed in DMSO and acetone mixtures of different proportions to detect the emissive response. It is obvious that the fluorescent intensity of **3** decreases with the addition of acetone (Fig. S6†). A similar quenching behavior of acetone has been reported previously.[37]

Aromatic compounds are widespread in refinery operations, plastic processing, and fuel operations, which are potentially neurotoxic and carcinogenic in nature. It is reported that Ln-MOFs have the potential of sensing aromatic molecules by host–guest interactions, which can be used to detect the aromatic compounds in the environment.[36] We investigated the chemical sensing of various nitrobenzene derivatives such as nitrobenzene (NB), 1,4-dinitrobenzene (DNB), 4-nitrophenylhydrazine (NPH), 4-nitroaniline (NA), *p*-nitrophenol (NP), 4-nitrotoluene (NT). Fig. 5d shows their fluorescence quenching percentage (QP) when the concentration of benzene derivatives is 0.13 mM in DMSO. The order of fluorescence quenching efficiency is NP > DNB > NPH > NA > NT > NB. The quenching percentage for NP is up to 75%, which is much higher than that for other nitrobenzene derivatives. Fig. 5c exhibits the decrease in fluorescence intensity of the dispersed solution of **3** in DMSO with the addition of 1 mM NP solution. To further reveal the quenching efficiency of NP, the Stern–Volmer equation, $(I_0/I) = K_{SV}[A] + 1$, was used to calculate the quenching constant (K_{SV}). Here, I_0 is the initial fluorescence intensity in the absence of the analyte and I is the fluorescence intensity after the addition of

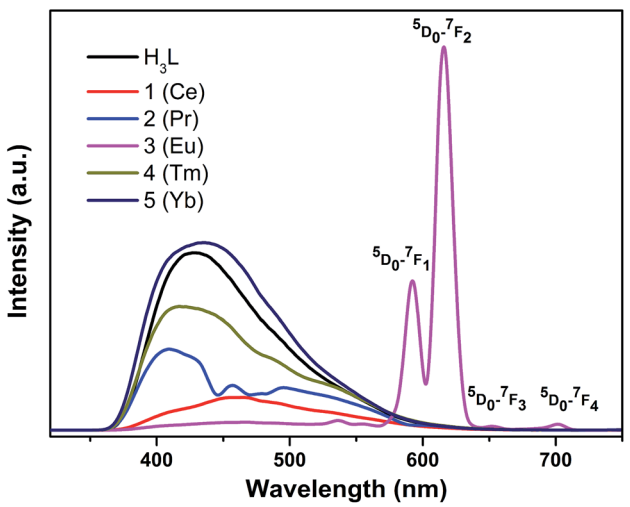

Fig. 4 Room-temperature emission spectra for free ligand and complexes **1–5**.

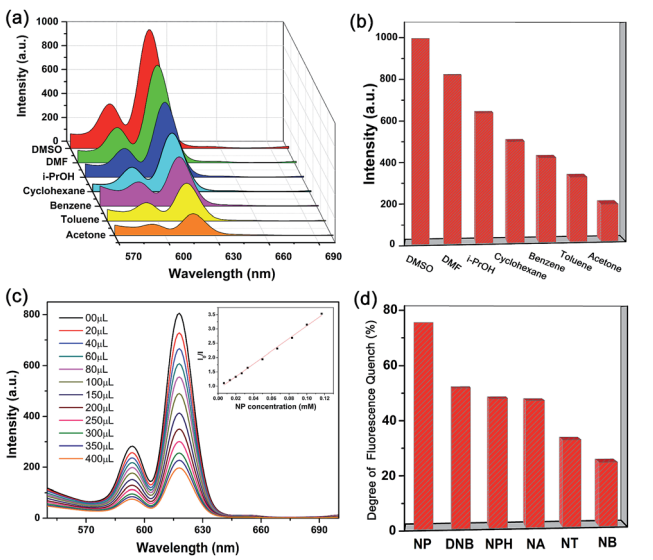

Fig. 5 (a) The PL spectra and (b) the $^5D_0 \rightarrow {}^7F_2$ transition intensities of the **3** (Eu) samples that were dispersed into various pure organic solvents. (c) Effect on the emission spectra of **3** (Eu) dispersed in DMSO upon incremental addition of a NP DMSO solution (1 mM). The legend indicates the overall concentration of NP. The Stern–Volmer plot of I_0/I *versus* the NP concentration is shown in the inset. (d) The degree of fluorescence quenches upon the addition of the nitrobenzene derivatives (0.13 mM).

the analyte. [A] is the concentration of the analyte.[81] The Stern–Volmer plot for NP is typically linear at low concentrations, and the value of K_{SV} for NP is estimated to be 2.2×10^4 M^{-1} (Fig. 5c). The results indicate a higher selectivity for NP, which is possible due to the presence of the OH– group. The highly acidic OH– group can interact strongly with the fluorophore *via* electrostatic interactions, and the quenching effect can be maintained over a long range due to the energy transfer mechanism.[36,82] Thus, the comprehensive reason with electrostatic interactions, favorable electrons, and the energy transfer mechanism results in a higher quenching effect.

Selective gas sorption properties

To investigate the permanent porosity of complexes **3–5**, the gas sorption experiments were measured. Considering that complexes **3–5** are isostructural, we chose **5** (Yb-MOF) as an example to study the permanent porosity. The as-synthesized **5** was guest-exchanged with dry methanol, followed by activation at 60 °C under high vacuum for 6 h to obtain the activated **5a**. The sorption isotherms for N_2, CO_2 and CH_4 are shown in Fig. 6a and b. It can be seen that the isotherms for CO_2 show the reversible Type-I, suggesting the retention of the microporous structure after the removal of guest molecules. The PXRD pattern of **5a** is consistent with that of the pristine sample, which also indicates that the structure is stable after the removal of the guest molecules (Fig. S5f†). At 77 K, no N_2 uptake was observed; however, CO_2 and CH_4 can be adsorbed at 273 K and 295 K. The uptakes of CO_2 are of 26.9 cm^3 g^{-1} at 273 K and 15.8 cm^3 g^{-1} at 295 K, which are much higher than those of CH_4 (6.04 and 3.36 cm^3 g^{-1}, at 273 and 295 K). It is obvious that complex **5** exhibits selective adsorption of CO_2 over N_2 and CH_4, although the adsorption amounts are somewhat lower than some reported results.[83–85] This is possibly attributed to the combined effects of the size of the pore and host–guest interactions. Complex **5** contains unsaturated Yb^{III} ions and π-electrons, which may generate an electric field to induce a dipole in CO_2. In addition, the interaction between the quadrupole moment of CO_2 and the electric field gradient further contributes to the adsorption potential energy of CO_2.[86–88] In addition, the isosteric heat (Q_{st}) of CO_2 can be calculated by fitting the CO_2 adsorption isotherms at 273 K and 295 K and it has the estimated value of 22.6 kJ mol^{-1}, which suggests the strong interactions between the CO_2 molecules and the coordination framework (Fig. 6c).[89]

To further investigate the CO_2 selectivity, the CO_2/CH_4 selectivity at 273 K was calculated by the ideal adsorbed solution theory (IAST) method. The predicted CO_2/CH_4 selectivities at mixture compositions for complex **5** were estimated by fitting the experimental single component isotherms using a single-site Langmuir–Freundlich model. As shown in Fig. 6d, the selectivities exhibit a decreasing trend in the range of 0–0.4 bar. A similar trend has been reported previously. The values of selectivity are all above 7.8, which are comparable with many reported MOFs.[84,90–92] Although the capture capacity of **5** for CO_2 is not particularly high, it exhibits exclusive capturing of CO_2 over a series of gases with high selectivity, indicating its potential applications in selective gas separation.

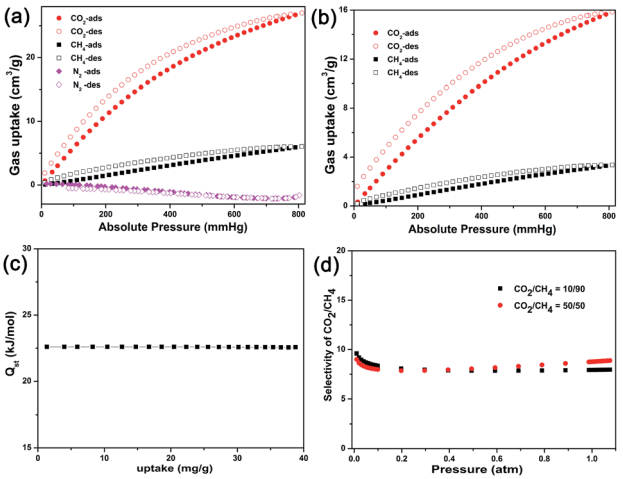

Fig. 6 (a) CO_2 and CH_4 adsorption capacity for **5** (Yb) at 273 K, and N_2 adsorption capacity at 77 K. (b) CO_2 and CH_4 adsorption capacity for **5** (Yb) at 295 K. (c) The Q_{st} of **5** (Yb) for CO_2. (d) The CO_2/CH_4 selectivity for **5** (Yb) at 273 K calculated by the IAST method for two CO_2 concentrations (CO_2/CH_4: 10/90 and 50/50) in CO_2/CH_4 binary mixtures.

Catalytic properties

Considering that complexes **3–5** have large channels and coordinative unsaturated metal sites, the cyanosilylation of aldehydes and ketones was chosen to test the catalytic properties of complex **5a**. The reaction is a convenient route to synthesize cyanohydrins, which can be used for both biological processes and synthetic chemistry.[93] A solution of aldehyde (0.5 mmol) and cyanotrimethylsilane (1 mmol) was added to complex **5a** (1.4 mol%), where cyanotrimethylsilane acted both as a reagent and as a solvent. Under a nitrogen atmosphere, the reaction mixture was stirred at room temperature, and the residual solution was analyzed by gas chromatography-mass spectrometry. As shown in Table 2, the conversion of benzaldehyde increases with increasing reaction time, and the yield reaches up to 99% for 24 h reaction. In comparison with previously reported Yb-MOFs (yield: 57%, 5 h), our catalyst exhibits higher conversion of benzaldehyde.[94] When a larger 1-naphthaldehyde

Table 2 Results for the cyanosilylation of aldehyde substrates in the presence of complex **5**

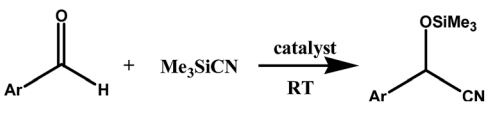

Entry	Time (h)	Ar	Yield (%)
1	5	Phenyl	66.9
2	12	Phenyl	84.5
3	24	Phenyl	99.0
4	24	Naphthyl	93.3
5	24	4-*tert*-Butylphenyl	56.2

was used, a relatively lower yield was obtained. The conversion decreases in the order benzaldehyde > 1-naphthaldehyde > *p-tert*-butyl benzaldehyde, which is attributed to the significant size-selectivity effect. In addition, recycling tests were measured over catalyst **5** for the cyanosilylation of benzaldehyde. The catalyst was easily filtered, washed, and recycled for three runs. Although a slightly decreased yield is observed, catalyst **5** still exhibits high activity (Fig. S7†).

Conclusions

In summary, five 3D Ln-MOFs were obtained based on a flexible carboxylate ligand. The structural diversity among **1–5** is attributed to the effects of lanthanide contraction and the different coordination modes of the organic ligand. The solid-state emission spectra of the complexes were investigated, where **3** shows the characteristic transitions of the Eu^{3+} energy-level structure, and the others have strong H_3**L**-based photoluminescent emission. It is worth noting that complex **3** shows a potential application for the luminescence sensing of small organic molecules, such as acetone and nitrobenzene derivatives. Complex **5** exhibits relatively permanent porosity and high selective adsorption of CO_2 over N_2 and CH_4, indicating the potential applications in selective gas separation. In addition, complex **5** has been successfully applied to catalyze the cyanosilylation of aldehydes, and exhibits comparatively high activity.

Acknowledgements

This work was supported by the NSFC (Grant nos 21271117, 21371179), NCET-11-0309, NSF of Shandong Province (BS2011CL041), and the Fundamental Research Funds for the Central Universities (13CX05010A, 13CX02006A).

Notes and references

1 O. M. Yaghi, M. O'Keeffe, N. W. Ockwig, H. K. Chae, M. Eddaoudi and J. Kim, *Nature*, 2003, **423**, 705–714.
2 S. Kitagawa, R. Kitaura and S. Noro, *Angew. Chem., Int. Ed.*, 2004, **43**, 2334–2375.
3 R. J. Kuppler, D. J. Timmons, Q. R. Fang, J. R. Li, T. A. Makal, M. D. Young, D. Q. Yuan, D. Zhao, W. J. Zhuang and H. C. Zhou, *Coord. Chem. Rev.*, 2009, **253**, 3042–3066.
4 H. C. Zhou, J. R. Long and O. M. Yaghi, *Chem. Rev.*, 2012, **112**, 673–674.
5 M. P. Suh, H. J. Park, T. K. Prasad and D. W. Lim, *Chem. Rev.*, 2012, **112**, 782–835.
6 J. R. Li, J. Sculley and H. C. Zhou, *Chem. Rev.*, 2012, **112**, 869–932.
7 Y. J. Cui, Y. F. Yue, G. D. Qian and B. L. Chen, *Chem. Rev.*, 2012, **112**, 1126–1162.
8 D. Zhao, D. Q. Yuan, D. F. Sun and H. C. Zhou, *J. Am. Chem. Soc.*, 2009, **131**, 9186–9188.
9 M. Zhang, G. Feng, Z. Song, Y. P. Zhou, H. Y. Chao, D. Yuan, T. Y. Tan, Z. Guo, Z. Hu and B. Z. Tang, *J. Am. Chem. Soc.*, 2014, **136**, 7241–7244.
10 M. Yoon, K. Suh, S. Natarajan and K. Kim, *Angew. Chem., Int. Ed.*, 2013, **52**, 2688–2700.
11 V. Stavila, A. A. Talin and M. D. Allendorf, *Chem. Soc. Rev.*, 2014, **43**, 10514–10518.
12 T. C. Narayan, T. Miyakai, S. Seki and M. Dincă, *J. Am. Chem. Soc.*, 2012, **134**, 12932–12935.
13 K. M. L. Taylor-Pashow, J. D. Rocca, Z. G. Xie, S. Tran and W. B. Lin, *J. Am. Chem. Soc.*, 2009, **131**, 14261–14263.
14 T. Kundu, S. Mitra, P. Patra, A. Goswami, D. Diaz and R. Banerjee, *Chem.–Eur. J.*, 2014, **6**, 3729–3738.
15 F. Ke, Y. P. Yuan, L. G. Qiu, Y. H. Shen, A. J. Xie, J. F. Zhu, X. Y. Tian and L. D. Zhang, *J. Mater. Chem.*, 2011, **21**, 3843–3848.
16 J. Liu, L. Chen, H. Cui, J. Zhang, L. Zhang and C. Y. Su, *Chem. Soc. Rev.*, 2014, **43**, 6011–6061.
17 K. Manna, T. Zhang and W. B. Lin, *J. Am. Chem. Soc.*, 2014, **136**, 6566–6569.
18 M. Yoon, R. Srirambalaji and K. Kim, *Chem. Rev.*, 2012, **112**, 1196–1231.
19 A. M. Shultz, O. K. Farha, J. T. Hupp and S. T. Nguyen, *J. Am. Chem. Soc.*, 2009, **131**, 4204–4205.
20 H. X. Deng, S. Grunder, K. E. Cordova, C. Valente, H. Furukawa, M. Hmadeh, F. Gándara, A. C. Whalley, Z. Liu, S. Asahina, H. Kazumori, M. O'Keeffe, O. Terasaki, J. F. Stoddart and O. M. Yaghi, *Science*, 2012, **336**, 1018–1023.
21 W. G. Lu, Z. W. Wei, Z. Y. Gu, T. F. Liu, J. Park, J. Tian, M. W. Zhang, Q. Zhang, T. Gentle, M. Bosch and H. C. Zhou, *Chem. Soc. Rev.*, 2014, **43**, 5561–5593.
22 D. Zhao, D. J. Timmons, D. Q. Yuan and H. C. Zhou, *Acc. Chem. Res.*, 2011, **44**, 123–133.
23 D. Q. Yuan, D. Zhao and H. C. Zhou, *Inorg. Chem.*, 2011, **50**, 10528–10530.
24 M. D. Allendorf, C. A. Bauer, R. K. Bhakta and R. J. T. Houk, *Chem. Soc. Rev.*, 2009, **38**, 1330–1352.
25 Q. Tang, Y. W. Liu, S. X. Liu, D. F. He, J. Miao, X. Q. Wang, G. C. Yang, Z. Shi and Z. P. Zheng, *J. Am. Chem. Soc.*, 2014, **136**, 12444–12449.
26 B. L. Chen, Y. Yang, F. Zapata, G. Lin, G. D. Qian and E. B. Lobkovsky, *Adv. Mater.*, 2007, **19**, 1693–1696.
27 S. S. Nagarkar, B. Joarder, A. K. Chaudhari, S. Mukherjee and S. K. Ghosh, *Angew. Chem., Int. Ed.*, 2013, **52**, 2881–2885.
28 H. L. Guo, Y. Z. Zhu, S. L. Qiu, J. A. Lercher and H. J. Zhang, *Adv. Mater.*, 2010, **22**, 4190–4192.
29 K. Sumida, D. L. Rogow, J. A. Mason, T. M. McDonald, E. D. Bloch, Z. R. Herm, T. H. Bae and J. R. Long, *Chem. Rev.*, 2012, **112**, 724–781.
30 P. Deria, J. E. Mondloch, E. Tylianakis, P. Ghosh, W. Bury, R. Q. Snurr, J. T. Hupp and O. K. Farha, *J. Am. Chem. Soc.*, 2013, **135**, 16801–16804.
31 M. Bu, C. P. Li, M. Chen, Z. W. Ge, X. Wang, L. Wang and C. S. Liu, *J. Am. Chem. Soc.*, 2014, **136**, 10906–10909.
32 D. M. Wang, T. T. Zhao, Y. Cao, S. Yao, G. H. Li, Q. S. Huo and Y. L. Liu, *Chem. Commun.*, 2014, **50**, 8648–8650.
33 P. S. Nugent, V. L. Rhodus, T. Pham, K. Forrest, L. Wojtas, B. Space and M. J. Zaworotko, *J. Am. Chem. Soc.*, 2013, **135**, 10950–10953.

34 J. H. Luo, J. Wang, G. H. Li, Q. S. Huo and Y. L. Liu, *Chem. Commun.*, 2013, **49**, 11433–11435.
35 P. Nugent, Y. Belmabkhout, S. D. Burd, A. J. Cairns, R. Luebke, K. Forrest, T. Pham, S. Q. Ma, B. Space, L. Wojtas, M. Eddaoudi and M. J. Zaworotko, *Nature*, 2013, **495**, 80–84.
36 X. Z. Song, S. Y. Song, S. N. Zhao, Z. M. Hao, M. Zhu, X. Meng, L. L. Wu and H. J. Zhang, *Adv. Funct. Mater.*, 2014, **24**, 4034–4041.
37 H. Li, W. Shi, K. Zhao, Z. Niu, H. Li and P. Cheng, *Chem.–Eur. J.*, 2013, **19**, 3358–3365.
38 A. V. S. Lourenco, C. A. Kodaira, E. R. Souza, M. C. F. Felinto, C. O. L. Malta and H. F. Brito, *Opt. Mater.*, 2011, **33**, 1548–1552.
39 C. Yan, K. Li, S. C. Wei, H. P. Wang, L. Fu, M. Pan and C. Y. Su, *J. Mater. Chem.*, 2012, **22**, 9846–9852.
40 B. L. Chen, L. B. Wang, F. Zapata, G. D. Qian and E. B. Lobkovsky, *J. Am. Chem. Soc.*, 2008, **130**, 6718–6719.
41 B. L. Chen, L. B. Wang, Y. Q. Xiao, F. R. Fronczek, M. Xue, Y. J. Cui and G. D. Qian, *Angew. Chem.*, 2009, **121**, 508–511.
42 P. Y. Wu, J. Wang, Y. M. Li, C. He, Z. Xie and C. Y. Duan, *Adv. Funct. Mater.*, 2011, **21**, 2788–2794.
43 P. Y. Wu, J. Wang, C. He, X. L. Zhang, Y. T. Wang, T. Liu and C. Y. Duan, *Adv. Funct. Mater.*, 2012, **22**, 1698–1703.
44 J. An, C. M. Shade, D. A. Chengelis-Czegan, S. Petoud and N. L. Rosi, *J. Am. Chem. Soc.*, 2011, **133**, 1220–1223.
45 J. Luo, H. Xu, Y. Liu, Y. Zhao, L. L. Daemen, C. Brown, T. V. Timofeeva, S. Ma and H. C. Zhou, *J. Am. Chem. Soc.*, 2008, **130**, 9626–9627.
46 T. Devic, O. David, M. Valls, J. Marrot, F. Couty and G. Férey, *J. Am. Chem. Soc.*, 2007, **129**, 12614–12615.
47 K. Binnemans, *Chem. Rev.*, 2009, **109**, 4283–4374.
48 B. D. Chandler, D. T. Cramb and G. K. H. Shimizu, *J. Am. Chem. Soc.*, 2006, **128**, 10403–10412.
49 N. L. Rosi, J. Kim, M. Eddaoudi, B. Chen, M. O'Keeffe and O. M. Yaghi, *J. Am. Chem. Soc.*, 2005, **127**, 1504–1518.
50 Y. P. He, Y. X. Tan and J. Zhang, *Inorg. Chem.*, 2013, **52**, 12758–12762.
51 H. Zhang, N. Li, C. Tian, T. Liu, F. Du, P. Lin, Z. Li and S. Du, *Cryst. Growth Des.*, 2012, **12**, 670–678.
52 T. Devic, O. David, M. Valls, J. Marrot, F. Couty and G. Ferey, *J. Am. Chem. Soc.*, 2007, **129**, 12614–12615.
53 D. X. Hu, F. Luo, Y. X. Che and J. M. Zheng, *Cryst. Growth Des.*, 2007, **7**, 1733–1737.
54 K. Ooi, Y. Tasaki-Handa, Y. Ade and A. Wakisaka, *Dalton Trans.*, 2014, 4807–4812.
55 Y. He, S. Xiang, Z. Zhang, S. Xiong, F. R. Fronczek, R. Krishna, M. O'Keeffe and B. Chen, *Chem. Commun.*, 2012, **48**, 10856–10858.
56 X. Yang, D. Schipper, R. A. Jones, L. A. Lytwak, B. J. Holliday and S. Huang, *J. Am. Chem. Soc.*, 2013, **135**, 8468–8471.
57 V. Chandrasekhar, P. Bag, M. Speldrich, J. van Leusen and P. Kogerler, *Inorg. Chem.*, 2013, **52**, 5035–5044.
58 F. N. Dai, D. Sun and D. F. Sun, *Cryst. Growth Des.*, 2011, **11**, 5670–5675.
59 R. Sun, S. Wang, H. Xing, J. F. Bai, Y. Z. Li, Y. Pan and X. Z. You, *Inorg. Chem.*, 2007, **46**, 8451–8453.
60 G. M. Sheldrick, *SHELXL-97, Program for X-ray Crystal Structure Refinement*, University of Gottingen, Gottingen, Germany, 1997.
61 A. L. Spek, *Implemented as the PLATON Procedure, a Multipurpose Crystallographic Tool*, Utrecht University, Utrecht, The Netherlands, 1998.
62 L. N. Jia, L. Hou, L. Wei, X. J. Jing, B. Liu, Y. Y. Wang and Q. Z. Shi, *Cryst. Growth Des.*, 2013, **13**, 1570–1576.
63 N. Wei, X. N. Zhang, G. M. Li, X. D. Zhang and Z. B. Han, *Cryst. Growth Des.*, 2014, **14**, 3002–3009.
64 S. Su, W. Chen, C. Qin, S. Song, Z. Guo, G. Li, X. Song, M. Zhu, S. Wang, Z. Hao and H. Zhang, *Cryst. Growth Des.*, 2012, **12**, 1808–1815.
65 M. Gustafsson, J. Su, H. J. Yue, Q. X. Yao and X. D. Zou, *Cryst. Growth Des.*, 2012, **12**, 3243–3249.
66 H. Y. Xu, F. H. Zhao, Y. X. Che and J. M. Zheng, *CrystEngComm*, 2012, **14**, 6869–6874.
67 Y. F. Han, X. H. Zhou, Y. X. Zheng, Z. Shen, Y. Song and X. Z. You, *CrystEngComm*, 2008, **10**, 1237–1242.
68 A. R. Ramya, S. Varughese and M. L. P. Reddy, *Dalton Trans.*, 2014, 10940–10946.
69 V. A. Blatov, *Topos*, 2007, http://www.topos.ssu.samara.ru.
70 A. L. Spek, *Acta Crystallogr., Sect. A: Found. Crystallogr.*, 1990, **46**, C34.
71 I. Persson, *Pure Appl. Chem.*, 2010, **82**, 1901–1917.
72 X. Zhou, Y. Guo, Z. Shi, X. Song, X. Tang, X. Hu, Z. Zhu, P. Li and W. Liu, *Dalton Trans.*, 2012, 1765–1775.
73 A. Niu, J. Yang, J. Guo, W. Q. Kan, S. Y. Song, P. Du and J. F. Ma, *Cryst. Growth Des.*, 2012, **12**, 2397–2410.
74 L. Wen, Z. Lu, J. Lin, Z. Tian, H. Zhu and Q. Meng, *Cryst. Growth Des.*, 2007, **7**, 93–99.
75 Z. J. Lin, L. W. Han, D. S. Wu, Y. B. Huang and R. Cao, *Cryst. Growth Des.*, 2013, **13**, 225–263.
76 N. M. Shavaleev, R. Scopelliti, F. Gumy and J. C. G. Bunzli, *Inorg. Chem.*, 2009, **48**, 2908–2918.
77 X. Yang, B. P. Hahn, R. A. Jones, K. J. Stevenson, J. S. Swinnea and Q. Wu, *Chem. Commun.*, 2006, 3827–3829.
78 J. Zhang, B. Zheng, T. Zhao, G. Li, Q. Huo and Y. Liu, *Cryst. Growth Des.*, 2014, **14**, 2394–2400.
79 X. Liu, X. Wang, T. Gao, Y. Xu, X. Shen and D. Zhu, *CrystEngComm*, 2014, **16**, 2779–2787.
80 Z. Chen, Y. Sun, L. Zhang, D. Sun, F. Liu, Q. Meng, R. Wang and D. Sun, *Chem. Commun.*, 2013, **49**, 11557–11559.
81 A. Ganguly, B. K. Paul, S. Ghosh, S. Kar and N. Guchhait, *Analyst*, 2013, **138**, 6532–6541.
82 S. S. Nagarkar, B. Joarder, A. K. Chaudhari, S. Mukherjee and S. K. Ghosh, *Angew. Chem., Int. Ed.*, 2013, **52**, 2881–2885.
83 Z. H. Xuan, D. S. Zhang, Z. Chang, T. L. Hu and X. H. Bu, *Inorg. Chem.*, 2014, **53**, 8985–8990.
84 B. Wang, H. Huang, X. L. Lv, Y. Xie, M. Li and J. R. Li, *Inorg. Chem.*, 2014, **53**, 9254–9259.
85 Y. Q. Chen, Y. K. Qu, G. R. Li, Z. Z. Zhuang, Z. Chang, T. L. Hu, J. Xu and X. H. Bu, *Inorg. Chem.*, 2014, **53**, 8842–8844.
86 L. Pan, K. M. Adams, H. E. Hernandez, X. Wang, C. Zheng, Y. Hattori and K. Kaneko, *J. Am. Chem. Soc.*, 2003, **125**, 3062–3067.

87 J. R. Li, R. J. Kuppler and H. C. Zhou, *Chem. Soc. Rev.*, 2009, **38**, 1477–1504.
88 R. R. Yun, J. G. Duan, J. F. Bai and Y. Z. Li, *Cryst. Growth Des.*, 2013, **13**, 24–26.
89 L. Czepirski and J. Jagiello, *Chem. Eng. Sci.*, 1989, **44**, 797–801.
90 Q. Yang, A. D. Wiersum, P. L. Llewellyn, V. Guillerm, C. Serre and G. Maurin, *Chem. Commun.*, 2011, **47**, 9603–9605.
91 W. Zhang, H. Huang, C. Zhong and D. Liu, *Phys. Chem. Chem. Phys.*, 2012, **14**, 2317–2325.
92 P. Xydias, I. Spanopoulos, E. Klontzas, G. E. Froudakis and P. N. Trikalitis, *Inorg. Chem.*, 2014, **53**, 679–681.
93 R. J. H. Gregory, *Chem. Rev.*, 1999, **99**, 3649–3682.
94 M. Gustafsson, A. Bartoszewicz, B. Martin-Matute, J. L. Sun, J. Grins, T. Zhao, Z. Y. Li, G. S. Zhu and X. D. Zou, *Chem. Mater.*, 2010, **22**, 3316–3322.